

## Simple Fabrication of Copper Nanoparticle-Loaded Biochar from Rosemary Extraction Residues for Peroxydisulfate Activation Towards Ponceau 4R Decolorization

Trang Thi Cam Tran<sup>1,2</sup>, Anh Thi Ngoc Phan<sup>1,2</sup>, Hung Minh Nguyen<sup>1,2</sup>, Long Quang Nguyen<sup>1,2</sup>, Tuyet-Mai Tran-Thuy<sup>1,2</sup>, Tien Xuan Le<sup>1,2</sup>, Dung Van Nguyen<sup>1,2\*</sup>

<sup>1</sup> Faculty of Chemical Engineering, Ho Chi Minh City University of Technology (HCMUT), 268 Ly Thuong Kiet Street, District 10, Ho Chi Minh City, Vietnam

<sup>2</sup> Vietnam National University Ho Chi Minh City, Linh Trung Ward, Thu Duc City, Ho Chi Minh City, Vietnam

\* Corresponding author's e-mail: [nvdung@hcmut.edu.vn](mailto:nvdung@hcmut.edu.vn)

### ABSTRACT

Rosemary extraction residues (RERs) are unused biomass released from the supercritical CO<sub>2</sub> extraction of rosemary essential oil. To reduce waste, RERs were used for the simple preparation of copper nanoparticle-loaded biochar (CuNPs/BC). One-pot pyrolysis of cupric acetate-impregnated RERs created zero-valent copper nanoparticles (CuNPs) with an average particle size of 15 ± 2 nm within the biochar (BC) matrix. Accordingly, the CuNPs/BC nanocomposite was applied for peroxydisulfate (PDS) activation in Ponceau 4R (P4R) decolorization. At 25 °C, initial pH 6.0, and 2.00 mM PDS, 1.00 g/L CuNPs/BC decolorized 99.3% P4R (20 ppm) after 120 min. Additionally, P4R decolorization was effective in a broad range of initial pH values (3.0–9.0). Altogether, RER-derived CuNPs/BC proved high potential for PDS activation towards P4R decolorization.

**Keywords:** rosemary extraction residue, copper nanoparticle, biochar, biomass valorization, one-pot synthesis, persulfate activation, Ponceau 4R.

### INTRODUCTION

Today, a variety of human activities and industrial processes discharge a large amount of organic pollutants into aquatic environments (Saravanan et al., 2021; Sousa et al., 2018). These pollutants include a wide range of compounds, such as pesticides, pharmaceuticals, surfactants, dyes, and organic solvents (Saxena et al., 2023; Saxena et al., 2020). Once in the water, organic pollutants can cause harmful impacts on both ecosystems and human health (Du et al., 2022; Mukhopadhyay et al., 2022). These contaminants can be toxic to aquatic organisms, disrupt their reproductive and growth processes, and diminish biodiversity. Human exposure to water contaminated with organic substances can lead to a range of health complications, such as cancer, hormonal disruptions, and developmental problems (Alharbi et al., 2018; Mishra et al., 2022). Although

some organic pollutants degrade quickly in natural environments, others resist degradation and accumulate in the food chain, posing long-term environmental and health risks (Rasheed et al., 2020; Titchou et al., 2021). Thus, effective remediation of organic contaminants is imperative prior to discharging them into aquatic environments (Nguyen et al., 2024).

Peroxydisulfate (S<sub>2</sub>O<sub>8</sub><sup>2-</sup>) is a versatile and potent oxidizing agent widely used to mitigate organic pollutants in water (Lee et al., 2020; Tian et al., 2022). Upon activation, PDS can generate highly reactive sulfate (SO<sub>4</sub><sup>•-</sup>) radicals, which can strongly degrade diverse organic contaminants. Hence, the effectiveness of PDS primarily depends on its activation to produce sulfate radicals. For that purpose, various activation methods, such as heat, UV radiation, electrical current, and transition metals, have been developed (Wang and Wang, 2022; Zhao et al., 2021). Among these

methods, PDS activation with transition metals (e.g., Fe, Co, and Cu) offers high performance, requires minimum energy, and reduces costs (Zheng et al., 2022). In practical applications, cobalt oxides cannot be used on large scales due to their toxicity (Hou et al., 2021a; Li et al., 2022a). Although zero-valent iron and iron oxides are commonly investigated for PDS activation, their performance is significantly reduced at high pH (Hou et al., 2021b; Karim et al., 2021). Different from Fe-based activators, zero-valent copper (Cu(0)) has the ability to activate PDS over a broad pH range (Li et al., 2022b). For example, Ni et al. (2023) reported that PDS was activated effectively by Cu(0) for Congo red treatment over a wide pH range of 3.0–11.0. Interestingly, Cu(0) particle sizes can affect the rate of Cu(I) leaching for PDS activation. Typical pH values for high degradation efficiencies of Congo red recorded from PDS activation by 15  $\mu\text{m}$  Cu(0) microparticles and 50 nm Cu(0) nanoparticles were 3.0 and 7.0, respectively. Similarly, Zhou et al. (2018) demonstrated that CuNPs showed high PDS activation performance towards degradation of 2,4-dichlorophenol over the initial pH range of 4.2–7.3. Despite possible advantages at the nanoscale, CuNPs are prone to agglomeration, which drastically reduces their reactivity (Kaittedanusorn et al., 2024; Wang et al., 2016). In order to prevent that phenomenon, it is necessary to immobilize CuNPs on appropriate supports.

Biochar is a carbon-rich material derived from the thermal decomposition of biomass in the absence of oxygen (Gupta et al., 2022; Qin et al., 2022). BC has gained attention not only for its role in carbon sequestration and soil amendment but also as a potential support (Cedeño et al., 2024; Pereira Lopes and Astruc, 2021). In fact, BC has a porous structure, surface functional groups, thermal stability, chemical stability, environmental compatibility, and low cost. Therefore, it could become a proper support for dispersion of CuNPs. Din et al. (2021) prepared a nanocomposite of BC and CuNPs through two steps. First, cotton stalks were pyrolyzed into BC. CuNPs were then dispersed on BC by a chemical reduction method. In general, that route required multisteps and  $\text{NaBH}_4$ , an expensive and toxic reducing agent. For industrial production, reducing steps can avoid lengthy processes and intermediate purification. Recent studies reported that one-pot pyrolysis of  $\text{FeCl}_3$ -impregnated biomass can easily generate iron oxides and zero-valent iron

particles within the BC matrix (Nguyen et al., 2023b; Nguyen et al., 2023c). The firm immobilization of these particles might enhance the stability and reusability of the composite (Feng et al., 2021). Based on that approach, this current study replaced  $\text{FeCl}_3$  with  $\text{Cu}(\text{CH}_3\text{COO})_2$ . The CuNPs formed might be fixed within the BC matrix, resulting in the CuNPs/BC composite.

Rosemary, scientifically known as *Rosmarinus officinalis*, is a typical shrub of the Mediterranean region with temperate climates (Mulas et al., 2002). The plant is also cultivated as an ornamental species in many areas of the world with warm climates (González-Minero et al., 2020). Aside from medicine and cooking purposes, rosemary is commonly used in the fragrance industry (Nguyen et al., 2023a; Sánchez-Camargo et al., 2016). For traditional production of rosemary essential oil, steam distillation and hydrodistillation are employed (Boutekedjiret et al., 2003). However, high operating temperatures can decompose and hydrolyze thermolabile compounds (Bensebia et al., 2009). In the case of organic solvent extraction, the essential oil can be restricted for the food processing industry, and its quality can be changed during solvent removal (Carvalho et al., 2005). Conversely, supercritical  $\text{CO}_2$  extraction can preserve natural components in rosemary essential oil, resulting in better antioxidant activity (Vicente et al., 2012; Yang et al., 2023). Regardless of the method used, a large amount of rosemary extraction residues (RERs) is released. RERs are normally collected and thrown away as waste with limited economic value (Bensebia et al., 2009). To valorize this underexploited biomass resource, RERs were used for the synthesis of CuNPs/BC through one-pot pyrolysis. The obtained material was subsequently explored for PDS activation towards Ponceau 4R decolorization.

## EXPERIMENTAL

### Materials

$\text{Cu}(\text{CH}_3\text{COO})_2 \cdot \text{H}_2\text{O}$  (99.0~102.0%),  $\text{NaOH}$  ( $\geq 96.0\%$ ),  $\text{H}_2\text{SO}_4$  (95.0~98.0%),  $\text{Na}_2\text{HPO}_4 \cdot 12\text{H}_2\text{O}$  ( $\geq 99.0\%$ ), and  $\text{Na}_2\text{S}_2\text{O}_3 \cdot 5\text{H}_2\text{O}$  ( $\geq 99.0\%$ ) were supplied from Xilong Scientific Co., Ltd. Other chemicals included Ponceau 4R from HiMedia Laboratories Pvt. Ltd.,  $\text{Na}_2\text{S}_2\text{O}_8$  ( $\geq 98.0\%$ ) from Shanghai Zhanyun Chemical Co., Ltd., and  $\text{KH}_2\text{PO}_4$  ( $\geq 99.5\%$ ) from Guangdong Guanghua

Sci-Tech Co., Ltd. Rosemary extraction residues were released from the supercritical CO<sub>2</sub> extraction of rosemary essential oil at a factory situated in Ho Chi Minh City, Vietnam. RERs were ground into a fine powder for further use.

### Synthesis of CuNPs/BC

Briefly, 5.00 g of RER powder and 1.00 g of Cu(CH<sub>3</sub>COO)<sub>2</sub> were introduced to 50.0 mL of distilled water. After stirring for 4.0 h, the mixture was dried at 105 °C for 24.0 h. Pyrolysis was conducted in a reactor under a nitrogen flow of 0.20 L/min. The temperature of the reactor was increased to 600 °C, with a heating rate controlled at 5 °C/min. Next, the pyrolysis temperature was kept constant for 60 min. The obtained CuNPs/BC sample was taken out and stored for later use. For comparison, BC was fabricated by direct pyrolysis of RER powder under the same conditions.

### Characterization of CuNPs/BC

Different advanced techniques were employed to determine the properties of CuNPs/BC. X-ray diffraction (XRD) was carried out on a Bruker D2 diffractometer with Cu-K $\alpha$  radiation ( $\lambda = 1.5418$  Å). Transmission electron microscopy (TEM) images were observed using a JEOL JEM-1010 instrument. Scanning electron microscope (SEM) images, energy dispersive X-ray (EDX) spectroscopy, and elemental mapping were obtained from a FE-SEM Hitachi S-4800 system, along with a Horiba EMAX 7593-H accessory. Fourier transform infrared (FTIR) spectroscopy was analyzed using a PerkinElmer Spectrum spectrometer.

### Ponceau 4R decolorization with PDS activated by CuNPs/BC

The PDS activation performance of CuNPs/BC was investigated for P4R decolorization at 25 °C. BC was used as a reference sample. Typically, 100 mL of P4R (20 ppm), a certain PDS dosage, and a certain CuNPs/BC dosage were prepared in each glass flask. Initial pH values were adjusted with H<sub>2</sub>SO<sub>4</sub> (0.1 M) and NaOH (0.1 M). During P4R treatment, the mixture was agitated using a magnetic stirrer. At each appropriate time, sampling was conducted, and the solid activator was promptly removed using a PTFE membrane filter (0.45  $\mu$ m). Then, the filtrate was added to a solution containing Na<sub>2</sub>S<sub>2</sub>O<sub>3</sub> and phosphate buffer

(pH 7.0). P4R concentrations were determined using a Jasco V-730 UV-Vis spectrophotometer at 507 nm. P4R decolorization (%) was calculated by the subsequent formula:

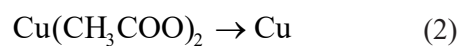
$$\text{P4R decolorization (\%)} = \frac{20 - C_t}{20} \times 100\% \quad (1)$$

The initial P4R concentration ( $C_0$ ) was 20 ppm, while  $C_t$  (ppm) was the remaining P4R concentration after  $t$  (min) of treatment.

## RESULTS AND DISCUSSION

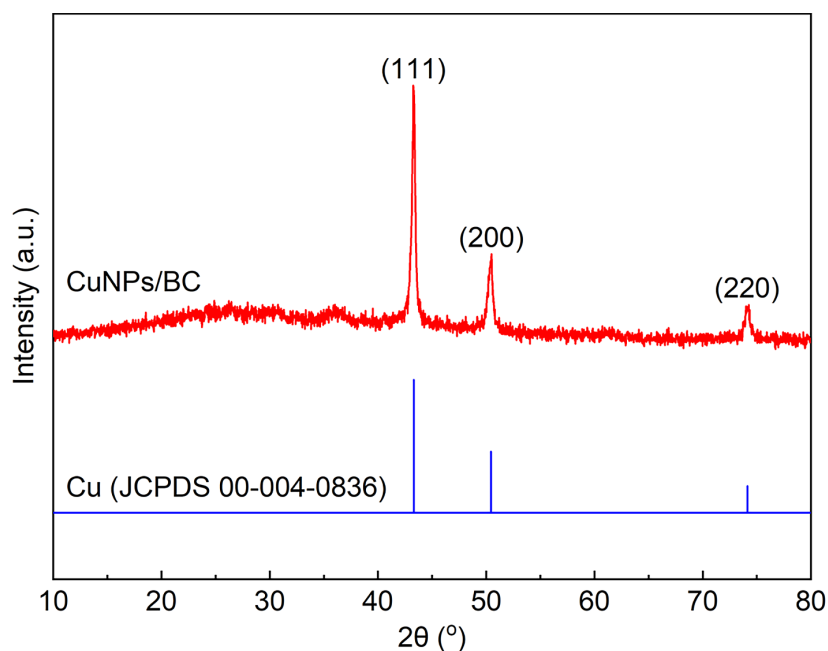
### Properties of CuNPs/BC

Figure 1 depicts the XRD pattern of CuNPs/BC. Sharp peaks recorded at  $2\theta = 43.3, 50.5,$  and  $74.1^\circ$  represent the 111, 200, and 220 planes of face-centered cubic Cu(0) crystals, respectively. However, the amorphous phase of BC possibly caused the noise baseline. Therefore, minor crystals were undetectable. This result proved that cupric acetate was converted to Cu(0) as the major product. The formation of Cu(0) within the BC matrix is anticipated by the following route:



During impregnation, aqueous cupric acetate could be dispersed within the RER structure. Under the nitrogen atmosphere, cupric acetate can be decomposed into Cu(0) at low temperatures (208–317 °C) (Sibokoza et al., 2021). Lignocellulosic biomass, which contains cellulose, hemicellulose, and lignin, has a wide temperature range for thermal decomposition (160–900 °C) (Pahnila et al., 2023; Yang et al., 2007). Therefore, heating cupric acetate-impregnated RERs could lead to the simultaneous decomposition of cupric acetate and carbonization of RERs. As a result, it is possible for Cu(0) particles to become entrapped within the BC matrix.

To clarify the structure of CuNPs/BC, its TEM images at the nanoscale are illustrated in Figure 2. The BC matrix is predictably exposed in bright areas. Conversely, darker dots that were broadly distributed in the composite could be CuNPs. In more detail, 20 CuNPs were counted using ImageJ software. As a result, CuNPs ranged between 10–20 nm with an average size of 15 nm and a standard deviation of 2 nm. In the impregnation step, cupric acetate might be located inside



**Figure 1.** XRD pattern of CuNPs/BC

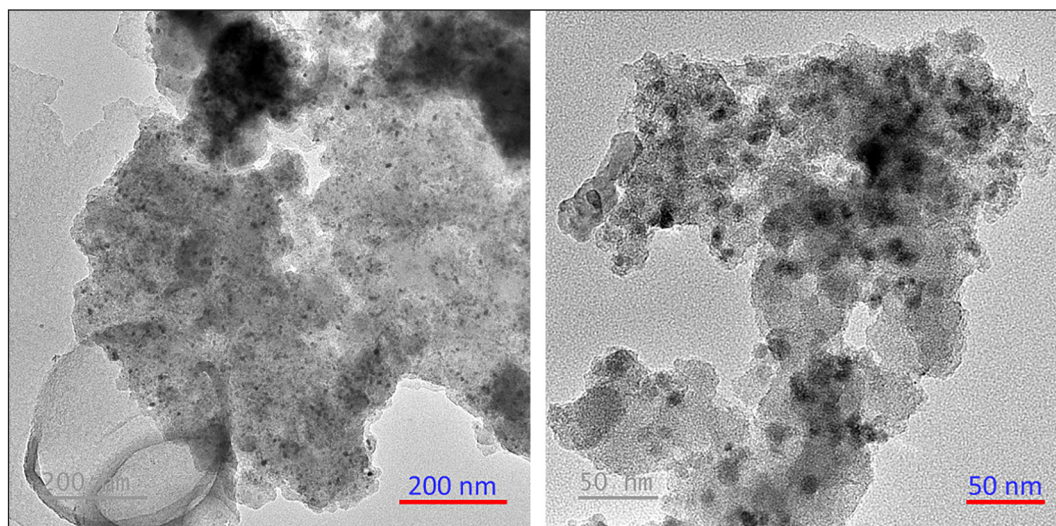


**Figure 2.** TEM images of CuNPs/BC

the empty spaces of the RER structure. During pyrolysis, the growth of CuNPs might be therefore limited in previously filled spaces, creating the nanocomposite structure of CuNPs/BC.

Figure 3 displays the surface morphology of CuNPs/BC. The material consists of fragments characterized by coarse and uneven surfaces. These fragments could be generated through grinding and pyrolysis steps. In a fragment, such cavities were also found, possibly originating from remnants of the RER structure. Generally, the surface texture of CuNPs/BC might affect its performance during use.

EDX spectroscopy and elemental mapping of CuNPs/BC were presented in Figure 4. The BC matrix was primarily constructed by C (71.70 wt%), while Cu (9.27 wt%) served as the dispersed phase. At the microscale, the uniform distribution of Cu within the nanocomposite was revealed by elemental mapping. Furthermore, 14.56 wt% O may exist in functional groups, metal oxides and salts. It is worth mentioning that trace elements including Mg, Al, K, Ca, Si, P, S, and Cl (0.13–2.05 wt%) may come from the RER resource. Indeed, rosemary has the ability to absorb minerals from the soil during its growth.

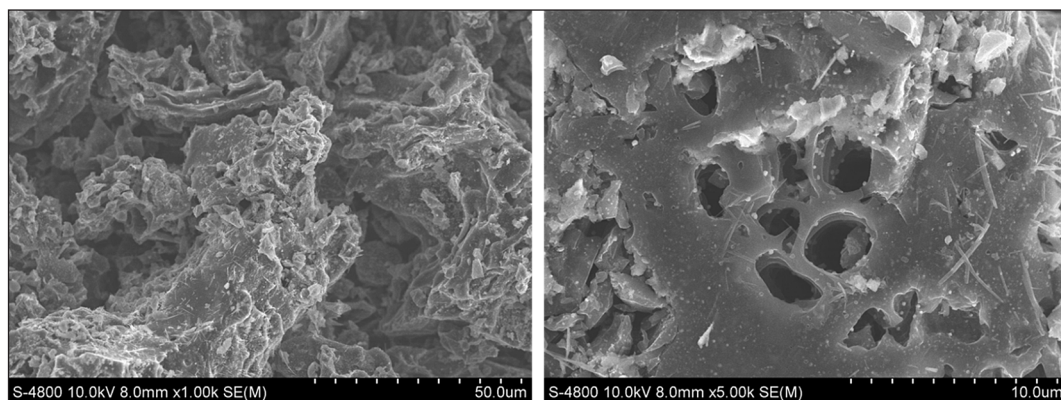


Figure 3. SEM images of CuNPs/BC

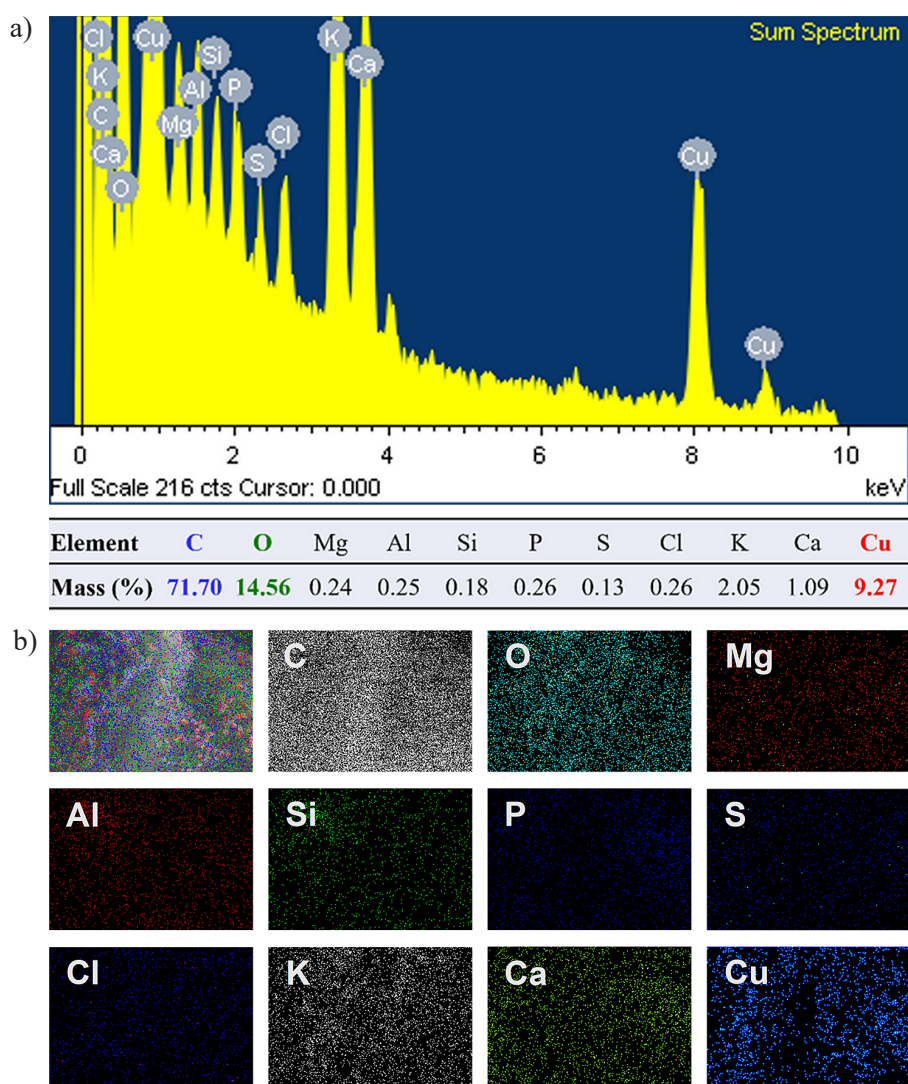


Figure 4. EDX spectroscopy (a) and elemental mapping (b) of CuNPs/BC

Consequently, these elements have the potential to be evenly dispersed in RERs, resulting in their homogeneous distribution in CuNPs/BC, as illustrated by elemental mapping.

As presented in Figure 5, CuNPs/BC contained such functional groups. An absorption peak at  $3060\text{ cm}^{-1}$  is assigned to O–H bonds, while a peak at  $1008\text{ cm}^{-1}$  could be the stretching

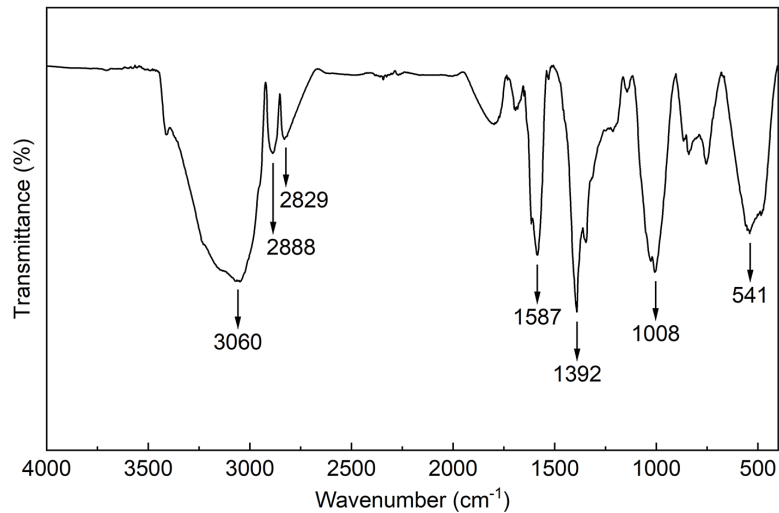


Figure 5. FTIR spectroscopy of CuNPs/BC

vibrations of C–O bonds. Moreover, C–H bonds could be recognized by peaks at 2888, 2829, and 1392  $\text{cm}^{-1}$ . Another peak at 1587  $\text{cm}^{-1}$  could be associated with aromatic C=C bonds. Notably, a peak at 541  $\text{cm}^{-1}$  might be the stretching vibrations of Cu–O bonds (Hua et al., 2023; Zayyoun et al., 2016) or minor minerals. Indeed, copper oxides might be formed during synthesis or storage in the air. Due to the presence of the aforementioned functional groups, the CuNPs/BC surface could become polarized, which is beneficial for its interaction with substances in water.

### Ponceau 4R decolorization with PDS activated by CuNPs/BC

As shown in Figure 6, P4R decolorization was tested using three systems: PDS alone, BC + PDS, and CuNPs/BC + PDS. Without any activator, PDS did not directly decolorize P4R, thereby highlighting the importance of PDS activation. However, the utilization of BC hardly enhanced P4R decolorization. Therefore, BC lacked the ability to activate PDS. Contrary to BC, CuNPs/BC triggered a gradual decrease in P4R concentration, ultimately eliminating 99.3% P4R after 120 min. This comparison indicated that CuNPs in the nanocomposite activated PDS into sulfate radicals for P4R decolorization. Based on prior research (Zhou et al., 2018), the activation mechanism of CuNPs/BC is suggested as follows:

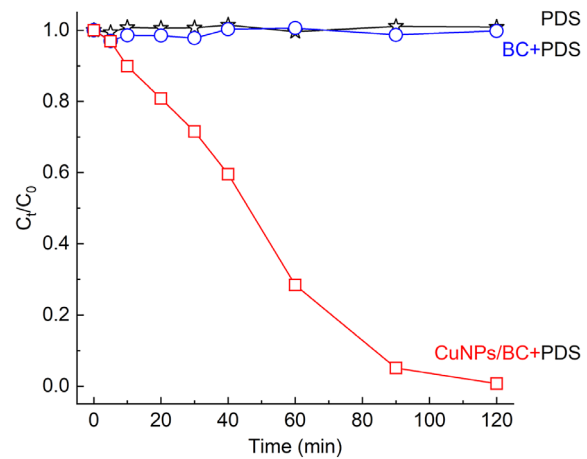
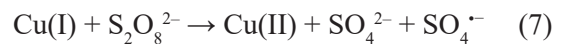
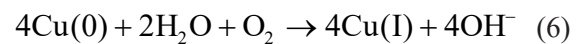
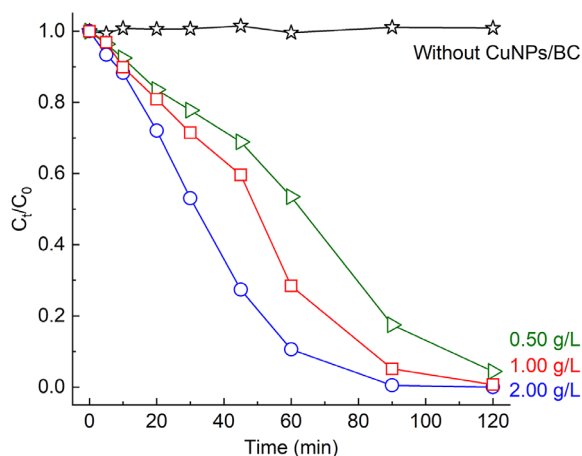


Figure 6. P4R decolorization with PDS activated by BC and CuNPs/BC (20 ppm P4R, 1.00 g/L activator, 2.00 mM PDS, pH 6.0)



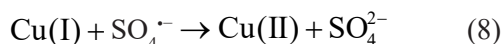
Cu(0) could be first oxidized into Cu(I) through Equations 4 to 6. The formed Cu(I) could then activate PDS into sulfate radicals (Equation 7). Thus, Cu(0) becomes a source of Cu(I) for PDS activation.

From practical considerations, the investigation of activator dosage in organic pollutant treatment with PDS is necessary. Unlike P4R decolorization without any activator, the addition of different CuNPs/BC dosages proved to be effective (Figure 7). As CuNPs/BC dosage increased from 0.50 to 2.00 g/L, P4R decolorization was accelerated gradually. As predicted, increasing CuNPs/



**Figure 7.** Effect of CuNPs/BC dosage on P4R decolorization with PDS (20 ppm P4R, 2.00 mM PDS, pH 6.0)

BC dosage could provide more active sites for higher production rates of sulfate radicals. However, excessive activator dosage could not only waste the activator but also potentially cause sulfate radical scavenging, as illustrated in Equation 8 (Deng et al., 2019).



PDS dosage plays an important role in the treatment efficiency of organic pollutants. Without PDS, CuNPs/BC hardly removed P4R. This result also indicated that the P4R adsorption capacity of CuNPs/BC was minimal. When PDS dosage increased from 1.00 to 5.00 mM, P4R decolorization was generally improved slightly. In fact, increasing PDS dosage could enhance the generation rate of sulfate radicals. However, the surplus use of PDS

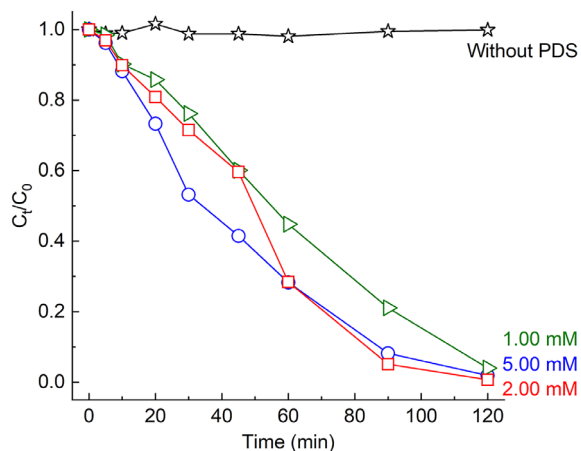


**Figure 8.** Effect of PDS dosage on P4R decolorization activated with CuNPs/BC (20 ppm P4R, 1.00 g/L CuNPs/BC, pH 6.0)

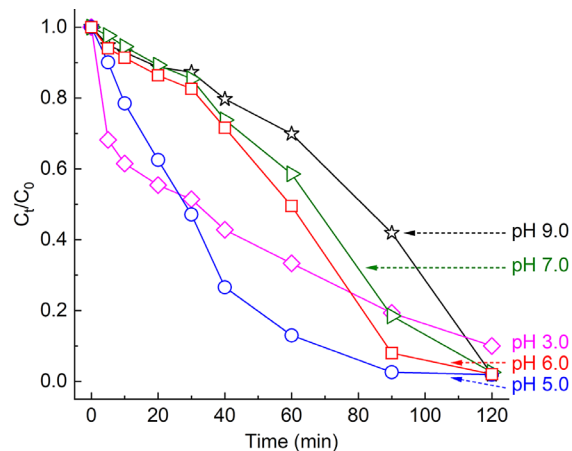
dosage may not be advantageous for P4R decolorization. As described in Equations 9 and 10, sulfate radicals could react with each other and PDS, reducing their availability for organic pollutant treatment (Lee et al., 2012, Lanhe et al., 2023).



Figure 9 depicts the influence of initial pH values (3.0–9.0) on P4R decolorization. In general, P4R decolorization decreased gradually as pH increased from 5.0 to 9.0. In acidic media, the corrosion process of Cu(0) into Cu(I) could be accelerated, according to Equation 11 (Zheng et al., 2022). Although an abundant Cu(I) quantity could lead to increased generation of sulfate radicals, the potential scavenging reactions mentioned before could consume them. Consequently, P4R decolorization at pH 3.0 showed a rapid rate in the first period but gradually slowed down in the later period.



When pH increased from 5.0 to 9.0, P4R decolorization became slower. High pH values could hamper the formation rate of Cu(I). Additionally, Cu(I) and Cu(II) could exist in precipitates, which might potentially cover the surface of CuNPs, preventing further corrosion (Deng et al., 2019; Zhou et al., 2018). Even so, P4R decolorization was still effective until pH 9.0. These results demonstrated that CuNPs could activate PDS over a wide pH range.



**Figure 9.** Effect of initial pH values on P4R decolorization with PDS activated by CuNPs/BC (20 ppm P4R, 1.00 g/L CuNPs/BC, 2.00 mM PDS)

## CONCLUSIONS

The current study successfully fabricated copper nanoparticle-loaded biochar via one-pot pyrolysis of cupric acetate-impregnated rosemary extraction residues under the nitrogen atmosphere. XRD and TEM results demonstrated that CuNPs with an average particle size of  $15 \pm 2$  nm were uniformly dispersed within the BC matrix. The CuNPs/BC nanocomposite was therefore investigated as a potential PDS activator for P4R decolorization. As a result, 99.3% P4R (20 ppm) was removed after 120 min of treatment with 2.00 mM PDS and 1.00 g/L CuNPs/BC at 25 °C and pH 6.0. In addition, P4R decolorization was efficient across a wide range of initial pH values, ranging from 3.0 to 9.0. These findings highlighted the potential of CuNPs/BC derived from RERs in activating PDS for P4R decolorization.

## Acknowledgments

We acknowledge Ho Chi Minh City University of Technology (HCMUT), VNU-HCM for supporting this study.

## REFERENCES

- Alharbi O.M.L., Basheer A.A., Khattab R.A. and Ali I. 2018. Health and environmental effects of persistent organic pollutants. *Journal of Molecular Liquids*, 263, 442–453.
- Bensebia O., Barth D., Bensebia B. and Dahmani A. 2009. Supercritical CO<sub>2</sub> extraction of rosemary: Effect of extraction parameters and modelling. *The Journal of Supercritical Fluids*, 49(2), 161–166.
- Boutekdjiret C., Bentahar F., Belabbes R. and Bessiere J.M. 2003. Extraction of rosemary essential oil by steam distillation and hydrodistillation. *Flavour and Fragrance Journal*, 18(6), 481–484.
- Carvalho R.N., Moura L.S., Rosa P.T.V. and Meireles M.A.A. 2005. Supercritical fluid extraction from rosemary (*Rosmarinus officinalis*): Kinetic data, extract's global yield, composition, and antioxidant activity. *The Journal of Supercritical Fluids*, 35(3), 197–204.
- Cedeño A., Olmo M., Cedeño G., Lucas M., Saldarriaga V. and Villar R. 2024. Effects of different biochar types on the growth and functional traits of rice (*Oryza sativa* L.). *Journal of Ecological Engineering*, 25(3), 282–290.
- Deng J., Xu M., Chen Y., Li J., Qiu C., Li X. and Zhou S. 2019. Highly-efficient removal of norfloxacin with nanoscale zero-valent copper activated persulfate at mild temperature. *Chemical Engineering Journal*, 366, 491–503.
- Din S.U., Awan J.M., Imran M., Zain-Ul-Abdin, Haq S., Hafeez M., Hussain S. and Khan M.S. 2021. Novel nanocomposite of biochar-zerovalent copper for lead adsorption. *Microscopy Research and Technique*, 84(11), 2598–2606. Du
- Y., Xu X., Liu Q., Bai L., Hang K. and Wang D. 2022. Identification of organic pollutants with potential ecological and health risks in aquatic environments: Progress and challenges. *Science of The Total Environment*, 806, 150691.
- Feng Z., Yuan R., Wang F., Chen Z., Zhou B. and Chen H. 2021. Preparation of magnetic biochar and its application in catalytic degradation of organic pollutants: A review. *Science of The Total Environment*, 765, 142673.
- González-Minero F.J., Bravo-Díaz L. and Ayala-Gómez A. 2020. *Rosmarinus officinalis* L. (rosemary): An ancient plant with uses in personal healthcare and cosmetics. *Cosmetics*, 7(4), 77.
- Gupta M., Savla N., Pandit C., Pandit S., Gupta P.K., Pant M., Khilari S., Kumar Y., Agarwal D., Nair R.R., Thomas D. and Thakur V.K. 2022. Use of biomass-derived biochar in wastewater treatment and power production: A promising solution for a sustainable environment. *Science of The Total Environment*, 825, 153892.
- Hou J., He X., Zhang S., Yu J., Feng M. and Li X. 2021a. Recent advances in cobalt-activated sulfate radical-based advanced oxidation processes for water remediation: A review. *Science of The Total Environment*, 770, 145311.
- Hou K., Pi Z., Yao F., Wu B., He L., Li X., Wang D., Dong H. and Yang Q. 2021b. A critical review on the mechanisms of persulfate activation by iron-based materials: Clarifying some ambiguity and controversies. *Chemical Engineering Journal*, 407, 127078.
- Hua L., Cheng T. and Wei T. 2023. Study on copper oxide modified biochar for activating persulfate high efficiency and application for the removal of bisphenol A. *Environmental Progress & Sustainable Energy*, 42(5), e14140.
- Kaittidanusorn N., Nagata T., Juthathan M., Tabaru K., Siengdung N., Pienpinijtham P., Tanaka T., Suzuki T., Tuntulani T., Leeladee P. and Obora Y. 2024. Facile and size-controllable fabrication of copper nanoparticles on nitrogen-doped carbon dots using an N,N-dimethylformamide-based reduction approach. *Results in Chemistry*, 7, 101398.
- Karim A.V., Jiao Y., Zhou M. and Nidheesh P.V. 2021. Iron-based persulfate activation process for environmental decontamination in water and soil. *Chemosphere*, 265, 129057.
- Lanhe Z., Chuan X., Zimeng L., Jingbo G., Guoguang D., Xin C. and Yanping J. 2023. Degradation

- of methyl orange using persulfate activated by magnetic CuS/Fe<sub>3</sub>O<sub>4</sub> catalyst: Catalytic performance and mechanisms. *Applied Surface Science*, 618, 156595.
18. Lee J., von Gunten U. and Kim J.-H. 2020. Persulfate-based advanced oxidation: Critical assessment of opportunities and roadblocks. *Environmental Science & Technology*, 54(6), 3064–3081.
  19. Lee Y.-C., Lo S.-L., Kuo J. and Lin Y.-L. 2012. Persulfate oxidation of perfluorooctanoic acid under the temperatures of 20–40 °C. *Chemical Engineering Journal*, 198–199, 27–32.
  20. Li B., Wang Y.-F., Zhang L. and Xu H.-Y. 2022a. Enhancement strategies for efficient activation of persulfate by heterogeneous cobalt-containing catalysts: A review. *Chemosphere*, 291, 132954.
  21. Li J., Liang Y., Jin P., Zhao B., Zhang Z., He X., Tan Z., Wang L. and Cheng X. 2022b. Heterogeneous metal-activated persulfate and electrochemically activated persulfate: A review. *Catalysts*, 12(9), 1024.
  22. Mishra A., Kumari M., Swati, Kumar R., Iqbal K. and Thakur I.S. 2022. Persistent organic pollutants in the environment: Risk assessment, hazards, and mitigation strategies. *Bioresource Technology Reports*, 19, 101143.
  23. Mukhopadhyay A., Duttagupta S. and Mukherjee A. 2022. Emerging organic contaminants in global community drinking water sources and supply: A review of occurrence, processes and remediation. *Journal of Environmental Chemical Engineering*, 10(3), 107560.
  24. Mulas M., Francesconi A.H.D., Perinu B. and Vais E.D. 2002. Selection of rosemary (*Rosmarinus officinalis* L.) cultivars to optimize biomass yield. *Journal of Herbs, Spices & Medicinal Plants*, 9(2–3), 133–138.
  25. Nguyen H.M., Tran A.T., Nguyen D.N.L., Lam H.H., Tran-Thuy T.-M., Nguyen L.Q., Le T.X. and Nguyen D.V. 2023a. One-pot fabrication of zero-valent iron-embedded activated carbon from rosemary distillation residues for malachite green removal. *Materials Research Express*, 10(8), 085603.
  26. Nguyen H.M., Truong T.B., Nguyen H.-H.T., Tran P.T., Tran-Thuy T.-M., Nguyen L.Q. and Nguyen D.V. 2023b. Catalytic ozonation of Ponceau 4R using multifunctional magnetic biochar prepared from rubber seed shell. *Journal of Ecological Engineering*, 24(12), 143–151.
  27. Nguyen L.T.K., Nguyen L.Q., Nguyen H.M., Nguyen T.M., Lam H.H., Tran-Thuy T.-M. and Nguyen D.V. 2023c. Simple one-step synthesis of nipa frond-derived magnetic porous carbon for decolorization of acid yellow 23. *Journal of Chemistry*, 2023, 5447693.
  28. Nguyen N.T.K., Le D.T.T., Vo K.D., Huynh L.T., Nguyen H.M., Tran-Thuy T.-M., Nguyen L.Q. and Nguyen D.V. 2024. Valorization of tropical almond (*Terminalia catappa*) leaves into iron-containing activated carbon for rapid catalytic degradation of methylene blue with hydrogen peroxide. *Journal of Ecological Engineering*, 25(8), 54–61.
  29. Ni X., Li Q., Yang K., Deng H. and Xia D. 2023. Efficient degradation of Congo red by persulfate activated with different particle sizes of zero-valent copper: performance and mechanism. *Environmental Science and Pollution Research*, 30(27), 70054–70064.
  30. Pahnla M., Koskela A., Sulasalmi P. and Fabritius T. 2023. A review of pyrolysis technologies and the effect of process parameters on biocarbon properties. *Energies*, 16(19), 6936.
  31. Pereira Lopes R. and Astruc D. 2021. Biochar as a support for nanocatalysts and other reagents: Recent advances and applications. *Coordination Chemistry Reviews*, 426, 213585.
  32. Qin F., Zhang C., Zeng G., Huang D., Tan X. and Duan A. 2022. Lignocellulosic biomass carbonization for biochar production and characterization of biochar reactivity. *Renewable and Sustainable Energy Reviews*, 157, 112056.
  33. Rasheed T., Shafi S., Bilal M., Hussain T., Sher F. and Rizwan K. 2020. Surfactants-based remediation as an effective approach for removal of environmental pollutants—A review. *Journal of Molecular Liquids*, 318, 113960.
  34. Sánchez-Camargo A.P., Mendiola J.A., Valdés A., Castro-Puyana M., García-Cañas V., Cifuentes A., Herrero M. and Ibáñez E. 2016. Supercritical anti-solvent fractionation of rosemary extracts obtained by pressurized liquid extraction to enhance their antiproliferative activity. *The Journal of Supercritical Fluids*, 107, 581–589.
  35. Saravanan A., Senthil Kumar P., Jeevanantham S., Karishma S., Tajsabreen B., Yaashikaa P.R. and Reshma B. 2021. Effective water/wastewater treatment methodologies for toxic pollutants removal: Processes and applications towards sustainable development. *Chemosphere*, 280, 130595.
  36. Saxena N., Islam M.M., Baliyan S. and Sharma D. 2023. A comprehensive review on removal of environmental pollutants using a surfactant based remediation process. *RSC Sustainability*, 1(9), 2148–2161.
  37. Saxena R., Saxena M. and Lochab A. 2020. Recent progress in nanomaterials for adsorptive removal of organic contaminants from wastewater. *Chemistry-Select*, 5(1), 335–353.
  38. Sibokoza S.B., Moloto M.J., Mtunzi F. and Moloto N. 2021. Thermal decomposition of copper acetate at various temperature and time to form copper oxide/copper nanoparticles. *Asian Journal of Chemistry*, 34(1), 239–244.
  39. Sousa J.C.G., Ribeiro A.R., Barbosa M.O., Pereira M.F.R. and Silva A.M.T. 2018. A review on

- environmental monitoring of water organic pollutants identified by EU guidelines. *Journal of Hazardous Materials*, 344, 146–162.
40. Tian K., Hu L., Li L., Zheng Q., Xin Y. and Zhang G. 2022. Recent advances in persulfate-based advanced oxidation processes for organic wastewater treatment. *Chinese Chemical Letters*, 33(10), 4461–4477.
  41. Titchou F.E., Zazou H., Afanga H., El Gaayda J., Ait Akbour R., Nidheesh P.V. and Hamdani M. 2021. Removal of organic pollutants from wastewater by advanced oxidation processes and its combination with membrane processes. *Chemical Engineering and Processing - Process Intensification*, 169, 108631.
  42. Vicente G., García-Risco M.R., Fornari T. and Reglero G. 2012. Supercritical fractionation of rosemary extracts to improve the antioxidant activity. *Chemical Engineering & Technology*, 35(1), 176–182.
  43. Wang B. and Wang Y. 2022. A comprehensive review on persulfate activation treatment of wastewater. *Science of The Total Environment*, 831, 154906.
  44. Wang J., Zhu H., Chen J., Zhang B., Zhang M., Wang L. and Du M. 2016. Small and well-dispersed Cu nanoparticles on carbon nanofibers: Self-supported electrode materials for efficient hydrogen evolution reaction. *International Journal of Hydrogen Energy*, 41(40), 18044–18049.
  45. Yang H., Yan R., Chen H., Lee D.H. and Zheng C. 2007. Characteristics of hemicellulose, cellulose and lignin pyrolysis. *Fuel*, 86(12), 1781–1788.
  46. Yang J., Goksen G. and Zhang W. 2023. Rosemary essential oil: Chemical and biological properties, with emphasis on its delivery systems for food preservation. *Food Control*, 154, 110003.
  47. Zayyoun N., Bahmad L., Laânab L. and Jaber B. 2016. The effect of pH on the synthesis of stable Cu<sub>2</sub>O/CuO nanoparticles by sol–gel method in a glycolic medium. *Applied Physics A*, 122(5), 488.
  48. Zhao Y., Yuan X., Li X., Jiang L. and Wang H. 2021. Burgeoning prospects of biochar and its composite in persulfate-advanced oxidation process. *Journal of Hazardous Materials*, 409, 124893.
  49. Zheng X., Niu X., Zhang D., Lv M., Ye X., Ma J., Lin Z. and Fu M. 2022. Metal-based catalysts for persulfate and peroxymonosulfate activation in heterogeneous ways: A review. *Chemical Engineering Journal*, 429, 132323.
  50. Zhou P., Zhang J., Zhang Y., Zhang G., Li W., Wei C., Liang J., Liu Y. and Shu S. 2018. Degradation of 2,4-dichlorophenol by activating persulfate and peroxymonosulfate using micron or nanoscale zero-valent copper. *Journal of Hazardous Materials*, 344, 1209–1219.